Flocculation behavior, mechanism, and optimization of tailings based on RSM-BBD-DF: Insight into the concentration and time-dependent floc size

Zhenqi Wang [1,4)], Aixiang Wu [1,4)], Zhuen Ruan [1,2,4*)], Raimund Bürger [3)], Shaoyong Wang [1,4)], Yi Mo [4,5)]

1) Key Laboratory of the Ministry of Education of China for High-efficient Mining and Safety of Metal Mines, University of Science and Technology Beijing, Beijing 100083, China

2) Shunde Innovation School, University of Science and Technology Beijing, Foshan 528399, China

3) CI^{2}MA and Departamento de Ingeniería Matemática, Facultad de Ciencias Físicas y Matemáticas, Universidad de Concepción, Casilla 160-C, Concepción, Chile

4) School of Civil and Resource Engineering, University of Science and Technology Beijing, Beijing 100083, China

5) China Railway Construction Tongguan Investment Co., Ltd, Tongling 244000, Anhui, China

*C**orresponding authors**: Zhuen Ruan, E-mail: ustb_ruanzhuen@hotmail.com

Abstract: Tailings thickening is the primary link and key technology of cemented paste backfill (CPB) technology, in which flocculation conditions are important factors affecting thickening effect. Conventional flocculation effects only consider macro indexes such as concentration and initial settling rate (ISR), ignoring the floc evolution. In this study, the multi-objective optimization of flocculation effect based on Response Surface Methodology-Box-Behnken Design-Desirability Function (RSM-BBD-DF) was carried out. Firstly, through the single-factor experiments, the sedimentation properties and floc size evolution under different influencing factors were analyzed. It is found that the evolution of floc size is time-dependent, which conforms to the Asym2sig model, and there is a linear relationship between test-ending floc size and ISR. The larger the floc, the higher the ISR. Through the RSM-BBD, the regression models of concentration and mean weighted chord length (MWCL) as response values were established. Multi-factors interaction found that the tailing feeding concentration (TFC) had the greatest influence on the concentration, and the shear rate (SR) had the greatest influence on the MWCL. The interaction between TFC and the flocculant solution concentration (FSC) has the highest influence on the concentration. The interaction between TFC and SR has the highest influence on the MWCL. By introducing the single Desirability Function and the overall Desirability Function, the optimization method based on RSM-BBD-DF obtained the optimal flocculation conditions, which were very close to the optimization results of Design Expert, indicating that RSM-BBD-DF optimization method is reliable. Thus, RSM-BBD-DF has important application value for multi-objective optimization in mining and other industries.

Keywords: Mean weighted chord length; Concentration; Time-dependent; Response Surface Methodology-Box-Behnken Design-Desirability function (RSM-BBD-DF)；Multi-objective optimization

1 Introduction

Cemented paste backfill (CPB) technology is a process that mixes tailings, waste rocks, cement, red mud, fly ash, and other cementing materials with water to backfill underground goafs. This technology offers advantages of safety, environmental friendliness, economy, and high efficiency, and can achieve the effect of "treating two hazards with one waste" [1-5]. CPB technology comprises four links: thickening, mixing, pipeline transportation, and stope maintenance. Among these, tailings thickening is the primary and key technology of CPB, and tailings thickening will form high concentration from low-concentration tailings slurry in thickeners [6-10]. Tailings undergo flocculation, sedimentation, dewatering, and consolidation in the thickener. Flocculation is the key process that determines the treatment capacity of the thickener, and tailings particles and flocculants are adsorbed and bridged on the upper part of thickeners to form larger flocs [11-14]. Flocs gather many tailings particles together to form large-size flocs, which greatly improves the processing efficiency of tailings. The flocculation effect is influenced by flocculant type, particle size distribution (PSD), tailing feeding concentration (TFC), flocculant solution concentration (FSC), flocculant unit consumption (FUC), shear rate (SR), and shear time (ST) [15-17]. With the continuous progress of mineral processing technology, tailings particles are becoming ever finer, which causes the problems of difficult flocculation and substandard concentration [15,18-20]. Therefore, it is of great significance to carry out research on ultrafine tailings flocculation.

Important indexes to measure the tailings flocculation effect include concentration and tailings processing capacity. The concentration reaching the standard is an important prerequisite to ensure CPB mixing and pipeline transportation [15,21]. Thickening efficiency mainly depends on whether the processing speed of the thickener can meet the requirements of continuous backfilling operation, among which tailings settling rate is the key index [15,22-24]. The settling rate is mainly related to the floc size, with larger flocs having a higher settling rate [25-26]. Many scholars have carried out research on flocs, but most of them are qualitative analyses of floc structure, lacking quantitative characterization of floc size. The structure of flocs (e. g. size and quantity) is a function of shearing time, and the floc evolution is highly time-dependent. Currently, research has not quantified the time-dependence of flocs evolution. Optical testing techniques such as Focused Beam Reflectance Measurement (FBRM) and Computed Tomography (CT) are commonly used for testing floc structure [15,27-30].

The influence of flocculation conditions on thickening effect is complex and diverse, and it results from multiple factors. Conventional single-factor experimental methods can only determine the optimal range, which has great

limitations for studying the interaction between multiple factors and the optimization of flocculation conditions under multiple objectives. Response Surface Methodology-Box-Behnken Design (RSM-BBD) can better avoid the shortcomings of the above experimental design methods and can carry out the analysis of main factor effects and interactions. RSM-BBD is a very reasonable experimental design method for the multi-factor and multi-objective optimization experiment of flocculation conditions [31-33]. Wu et al. [15] conducted a study on the optimization of flocculation conditions based on BBD, and obtained the optimal flocculation conditions. Panda et al. [34] used BBD to study the effects of flocculant dosage, dispersant dosage, pH, and other flocculating conditions on the chromium tailings during flocculation. Arjmand [35] also used BBD to study the effects of FUC (5-20 g t^{-1}), TFC (3-12 wt%), pH (4-12), and FSC (0.05-1 wt%) on thickening performance (settling rate, turbidity, and concentration). Yin et al. [36] used the orthogonal test scheme to carry out a settling column test on fine-grained unclassified tailings, analyzed the influence of unclassified tailings concentration, FUC, and FSC on concentration and settling rate, and obtained the optimal flocculation conditions.

The indexes used to measure the thickening effect include concentration, initial settling rate, and turbidity [15]. However, most current studies aim to optimize flocculation conditions for a single response value. Qi et al. [37] used a machine learning method to analyze and optimize the influence of 17 variables on the ISR. Pedersen et al. [38] conducted experiments on the ISR of ultra-fine tailings under different FUCs, pHs, and temperatures. Niu et al. [39] conducted experiments on the ISR of ultra-fine tailings under different flocculant dosages, pHs, and temperatures. However, no multi-objective optimization of flocculation conditions has been carried out, which makes the obtained flocculation conditions one-sided. Using MATLAB to carry out multi-objective optimization is an important method. Furthermore, the Desirability Function (DF) is also an effective multi-objective optimization method. By giving different response values corresponding weights for analysis, optimal flocculation conditions can be obtained [40-42].

In this study, we first analyzed the evolution of concentration, ISR, and Mean Weighted Chord Length (MWCL) under single-factor flocculation conditions. We quantitatively characterized the time dependence of floc size and analyzed the evolution mechanism of floc size with shearing time. We also quantitatively characterized the ISR-MWCL relationship. Through single-factor experiments, we obtained the reasonable range of each flocculation condition. We then carried out experiments based on RSM-BBD, established corresponding multivariate nonlinear regression models, and analyzed the interaction of flocculation factors. Finally, we obtained the optimal flocculation conditions based on the RSM-BBD-DF multi-objective optimization method.

2 Materials and methods

2.1 Raw materials

2.1.1 Tailings

The tailings used in this study come from a lead-zinc mine in China. Based on different particle sizes, the tailings can be divided into coarse-grained tailings (classified tailings) and fine-grained tailings (ultrafine tailings). The unclassified tailings comprise 30 wt% fine-grained tailings and 70 wt% coarse-grained tailings. The PSD was analyzed by OMEC laser particle size analyzer [1,5], and the results are shown in Fig. 1.

As shown in Fig. 1, the particle size of ultrafine tailing does not exceed 100 μm, with a particle size range of 0.1-60 μm. The proportion less than 10 μm is more than 50 vol% and C_c (0.9) is less than 1, indicating that it belongs to fine-grained tailings. The particle size of classified tailings ranges from 1-400 μm, with the proportion more than 100 μm being over 30 vol%, the C_u (4.7) is less than 5, indicating that it belongs to coarse-grained tailings. The particle size of unclassified tailings ranges from 0.1-400 μm.

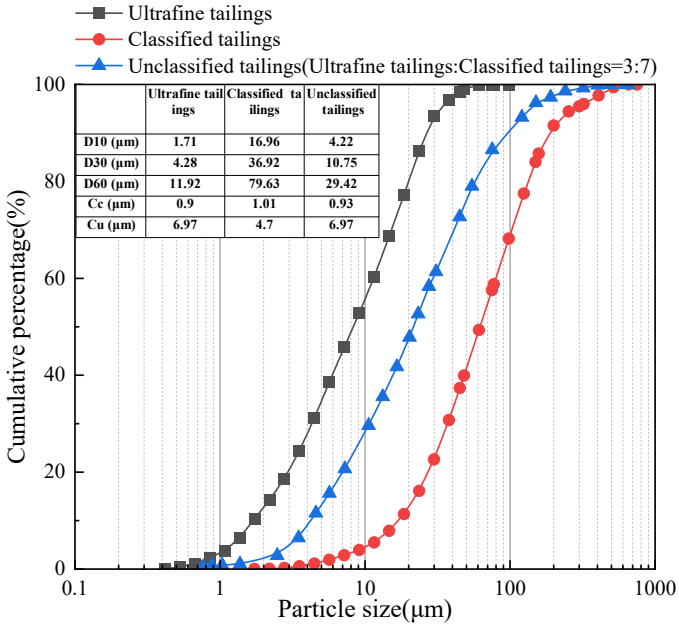

	Ultrafine tailings	Classified tailings	Unclassified tailings
D10 (μm)	1.71	16.96	4.22
D30 (μm)	4.28	36.92	10.75
D60 (μm)	11.92	79.63	29.42
Cc (μm)	0.9	1.01	0.93
Cu (μm)	6.97	4.7	6.97

Fig. 1 Tailings particle size distribution

The specific gravity of fine-grained tailings and coarse-graded tailings was measured by the pyknometer method. The specific gravity of fine-grained tailings is 3.063, and that of coarse-grained tailings is 3.008. The porosity and specific surface area (SSA) of fine-grained tailings and coarse-grained tailings were analyzed. The loose porosity of fine-grained tailings is 67.14%, the dense porosity is 59.09%, and the SSA is 1405.60 $m^2 \cdot kg^{-1}$. The loose porosity of the coarse-grained tailings is 52.52%, the dense porosity is 40.16%, and the SSA is 172.86 $m^2 \cdot kg^{-1}$.

X-ray Fluorescence (XRF) was used to analyze the chemical components of fine-grained and coarse-grained tailings. As shown in Table 1, both fine-grained tailings and coarse-grained tailings contain high levels of CaO and MgO.

Table 1 Chemical composition of fine-grained tailings and classified tailings (wt%)

	CaO	MgO	SiO2	Al2O3	Fe	S	Zn	Pb
Fine-grained tailings	38.62	6.63	6.17	2.8	2.29	2.02	1.05	0.96
Coarse-grained tailings	31.26	12.45	4.68	1.79	2.97	1.25	2.43	1.17

2.1.2 Flocculant

SNF polyacrylamide (PAM) suitable for the thickening of mine tailings was selected, including one type of cationic polyacrylamide (CPAM) 350E, one type of nonionic polyacrylamide (NPAM) 6003S, and three types of anionic polyacrylamides (APAM) 625S, 645S, and 665S. The main difference among the PAMs is the molecular weight (Table 2), with 665S having the highest molecular weight, followed by 645S, 625S, 6003S, and 350E having the lowest molecular weight.

Table 2 PAM types and molecular weight

	CAPM	APAM			NPAM
Type	350E	625S	645S	665S	6003S
molecular weight ($\times 10^4$)	700	1100	1100	1300	1000

2.1.3 Experimental water

The water used in experiments is filtered tap water from the laboratory, and its pH is 7.0.

2.2 Experimental methods

This research experiment is divided into two stages. In the first stage, single-factor flocculation experiments were conducted to determine the reasonable range of each influencing factor. Based on the factor range, multi-factor flocculation conditions optimization was carried out using RSM-BBD-DF.

2.2.1 Single-factor flocculation experiment

The study was conducted using the flocculation experimental device shown in Fig. 2. The MWCL during flocculation was tested by FBRM [15]. Meanwhile, the ISR was tested by settling column experiments [15]. Concentration is one of the most important indexes for measuring the thickening effect.

The single-factor flocculation experiment mainly studies the influence of PAM type, TFC, FSC, SR, and ST on MWCL, ISR, and concentration. The PAMs were described in Section 2.1.2. Then, the single-factor flocculation experiment was carried out according to the scheme in Table 3. The TFCs are 5, 10, 15, 20, and 25 wt%. The FSCs are 0.01, 0.0325, 0.055, 0.0775, and 0.1 wt%. The SRs are 80, 160, 240, 320, and 400 $r \cdot min^{-1}$. The STs are 30, 60, 90, 120, and 150 s. The experiments were carried out using the experimental device shown in Fig. 2. The specific experimental process is as follows:

(1) The tailings slurry was prepared according to the experimental scheme, and a mixer (IKA EUROSTAR 60 digital) was used to mix the tailings. Then, FBRM was used to test the floc size evolution. The portable Particle Track G400 was used with iC FBRM for data acquisition and transformation [43-44]. The sampling period was 2 s.

(2) Pour the tailings slurry after FBRM test into the settling cylinder for settling column experiments [45]. Shoot the settling process with a high-speed camera, record the change of the solid-liquid interface height with settling time through playback of the video, and obtain the ISR through fitting the solid-liquid interface height-shearing time (0-60 s) straight line. The absolute slope value is ISR. The measuring range of the settling column cylinder is 1000 ml. After settling for 24 h, the concentration was tested.

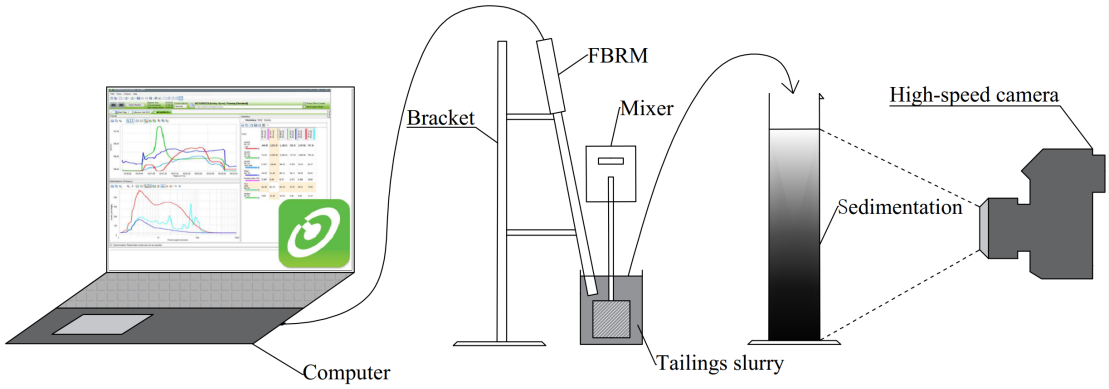

Fig. 2 Experimental process and methods

Table 3 Single-factor experimental scheme

	TFC (wt%)	FSC (wt%)	SR (r·min^{-1})	ST (s)
TFC (wt%)	5, 10, 15, 20, 25	15	15	15
FSC (wt%)	0.1	0.01, 0.0325, 0.055, 0.0775, 0.1	0.1	0.1
SR (r·min^{-1})	240	240	80, 160, 240, 320, 400	240
ST (s)	90	90	90	30, 60, 90, 120, 150

2.2.2 Multi-factor flocculation conditions optimization

Based on the RSM-BBD, this experiment conducts optimization research of flocculation conditions with four factors and three levels. The experimental factors and levels are shown in Table 4. Taking TFC, FSC, SR, and ST as experimental factors, the TFC ranges from 10 to 25 wt%, FSC ranges from 1 to 10 wt‰, SR ranges from 80 to 400 r·min^{-1}, and ST ranges from 30 to 150 s. The floc size affects the ISR [25,29-30,46-47]. The larger the floc size, the higher the thickening efficiency. At the same time, the concentration is an important raw material for the subsequent mixing and pipeline transportation of the CPB system. Therefore, the MWCL and concentration are taken as the two response values to optimize the flocculation condition, and there are 29 experimental groups.

This experiment also uses the flocculation and sedimentation experimental device shown in Fig. 2 to test the floc size (MWCL) and concentration.

Table 4 RSM-BBD experimental factors and levels

Factors	Unit	-1	0	1
TFC-x_1	wt%	10	17.5	25

FSC-x_2	wt‰	1	5.5	10
SR-x_3	r·min^{-1}	80	240	400
ST-x_4	s	30	90	150

3 Results and discussion

3.1 Influence of single factor on flocculation

3.1.1 Influence of PAM types on flocculation

Under different PAM types, the solid-liquid interface first drops rapidly, then slowly, and finally remains stable with settling time (Fig. 3(a)). PAMs 625S, 645S, 665S, 350E, and 6003S have corresponding ISRs of 2.00, 2.22, 1.31, 1.00, and 1.34 mm·s^{-1}, respectively. APAM 645S has the highest ISR, while CPAM 350E has the lowest ISR.

Fig. 3(b) shows that the MWCL of APAM 645S is higher than that of other PAMs, and the MWCL at the end of shearing (Shearing time 90 s) is also the highest. The MWCL quickly increases to the peak, then slowly decreases, and finally stabilizes. In the rapid growth stage, tailings particles are mainly combined with PAMs. After the peak, large-size flocs are broken and reconstructed into small-size flocs under the mixer-shearing action. Finally, they reach the dynamic process of breaking and reconstruction, which tends to be stable. Thus, the evolution of floc size is time-dependent. Different PAMs react with different times to reach the peak, among which CPAM 350E takes longer to reach the peak than APAMs and NPAM, while NPAM 6003S takes the shortest time to reach the peak. The growth-rupture-reconstruction process of flocs conforms to the Peak Function [48-49]. Parallel multi-step process deconvolution usually utilizes the Asymmetric Double Sigmoidal (Asym2sig). Therefore, the Asym2sig normal distribution model of Eq. (1) is used for fitting analysis. The fitting curve is closely related to the data points, which can reflect the time dependence of floc size evolution. The t_c in the equation can determine the shearing time reaching the peak value. Supporting Information (Table S1) shows the t_c value of 350E is the highest (56.66), and that of 6003S is the lowest (5.066), which is consistent with the shearing time reaching the peak in Fig. 3(b). Therefore, the model can analyze the time-dependent property of floc size evolution.

$$L = l_0 + A \cdot \frac{1}{1+e^{-\frac{t-t_c+w_1/2}{w_2}}} \cdot \left(1 - \frac{1}{1+e^{-\frac{t-t_c-w_1/2}{w_3}}}\right) \quad (1)$$

Where L is the MWCL, μm; t is the shearing time, s; l_0 is the initial value of the Asym2sig function at t_0, μm; A, t_c, w_1 are maximum amplitude, center, and width of the curve, respectively; w_2, and w_3 are shape parameters to determine the peak position; $w_1 > 0$, $w_2 > 0$, $w_3 > 0$.

Fig. 3(c) shows that the concentration corresponding to APAM 645S is the highest (48.54 wt%), and that corresponding to CPAM 350E is the lowest (31.99 wt%). The above results show that APAM 645S is the best, with the highest ISR,

concentration, and MWCL. Therefore, APAM 645S is the best for flocculation and sedimentation experiments.

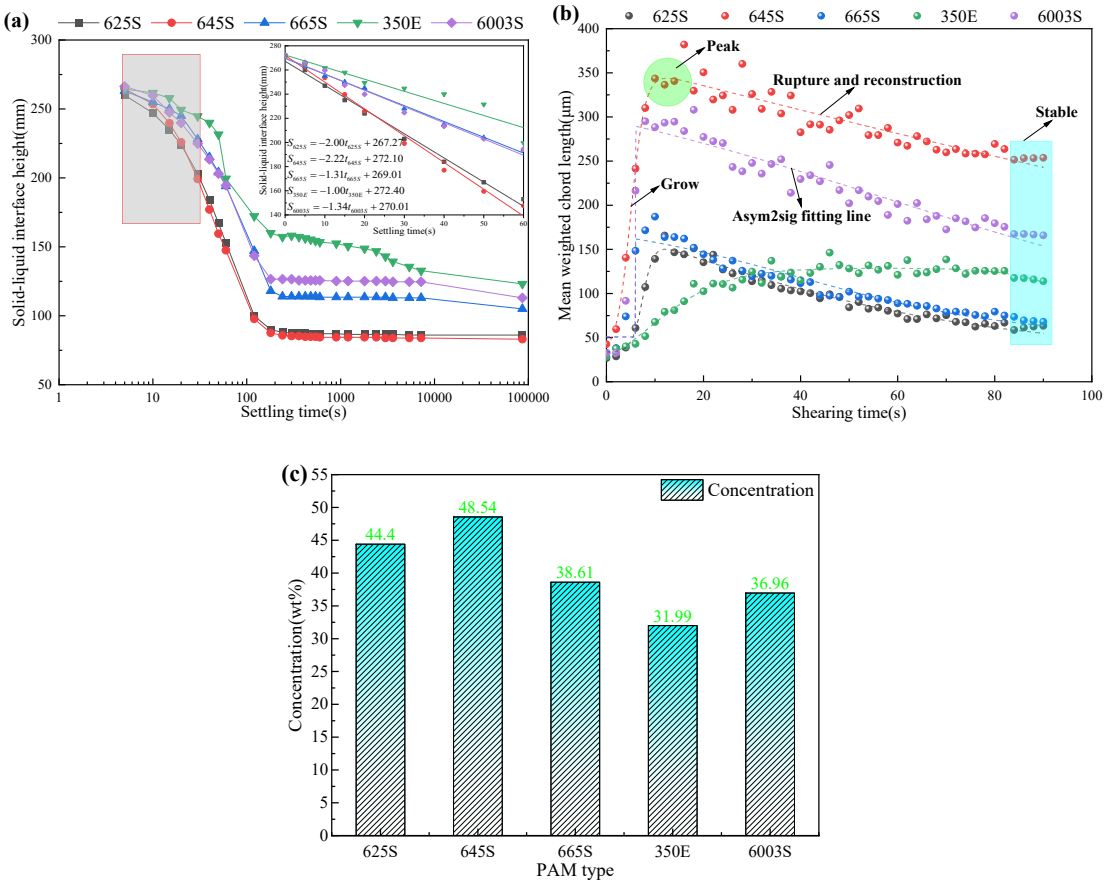

Fig. 3 Flocculation, sedimentation and consolidation properties under different PAMs: (a) Settling curves; (b) Floc size evolution; (c) Concentration

3.1.2 Influence of TFC on flocculation

With the increase of TFC, the settling curve moves up continuously (Fig. 4(a)). The ISRs corresponding to TFCs of 5, 10, 15, 20, and 25 wt% are 3.86, 3.61, 2.07, 1.21, and 0.35 mm·s^{-1}, respectively. As TFC increases, the ISR decreases continuously.

With the increasing TFC, the MWCL evolution curves move down continuously, indicating that the higher the TFC, the smaller the flocs (Fig. 4(b)). The MWCLs with different TFCs at the end of testing are 299.815, 284.006, 255.612, 166.952, and 97.048 μm. With the continuous increase of TFC, the MWCL increases. The floc size evolution curves corresponding to different TFCs also conform to Asym2sig models (Table S1).

Fig. 4(c) shows that the concentrations corresponding to TFCs are 51.48, 41.28, 45.93, 41.76, and 41.03 wt%, respectively. With the continuous increase of TFC, the concentration shows a decreasing trend. Since the tailings treatment efficiency of 5 wt% TFC is low and cannot meet the requirements of industrial production, it is suggested that the reasonable range of TFC is 10-25 wt%.

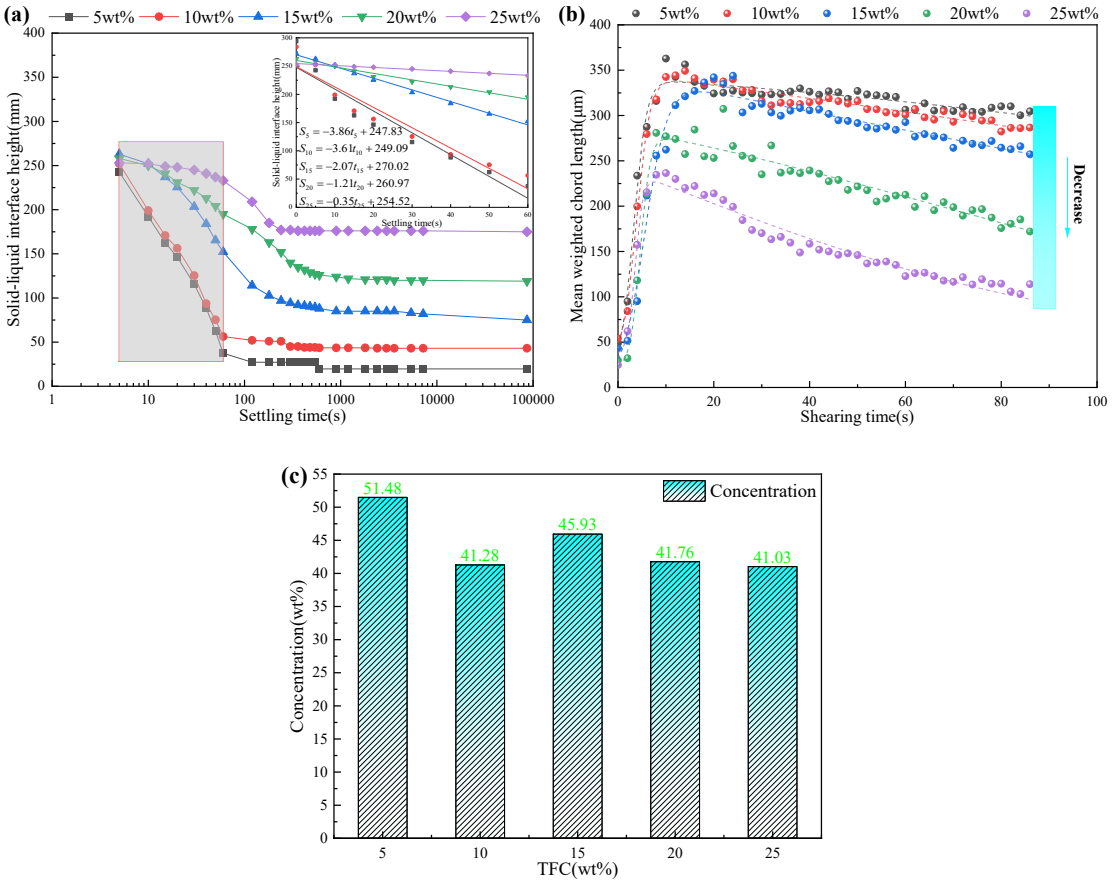

Fig. 4 Flocculation, sedimentation, and consolidation properties under different TFCs: (a) Settling curves; (b) Floc size evolution; (c) Concentration

3.1.3 Influence of FSC on flocculation

With the increase of FSC, the settling curve moves up continuously (Fig. 5(a)). The ISRs of FSCs 0.01, 0.0325, 0.055, 0.0775, and 0.1 wt% are 2.71, 2.67, 2.07, 1.38, and 0.95 mm·s^{-1}, respectively. With the increase of FSC, the ISR decreases continuously.

The MWCL of flocs corresponding to different FSCs at the shearing time of 90 s is 274.039, 265.612, 255.610, 243.805, and 232.092 μm, respectively (Fig. 5(b)). This law also reveals why the ISR is low when the FSC is high. The floc evolution curves corresponding to different FSCs conform to Asym2sig models (Table S1).

Fig. 5(c) shows that the concentrations corresponding to different FSCs are 48.9, 46.7, 45.93, 44.84, and 39.82 wt%, respectively. With the continuous increase of FSC, the concentration keeps decreasing. To sum up, the reasonable range of FSC is 0.01-0.1 wt%.

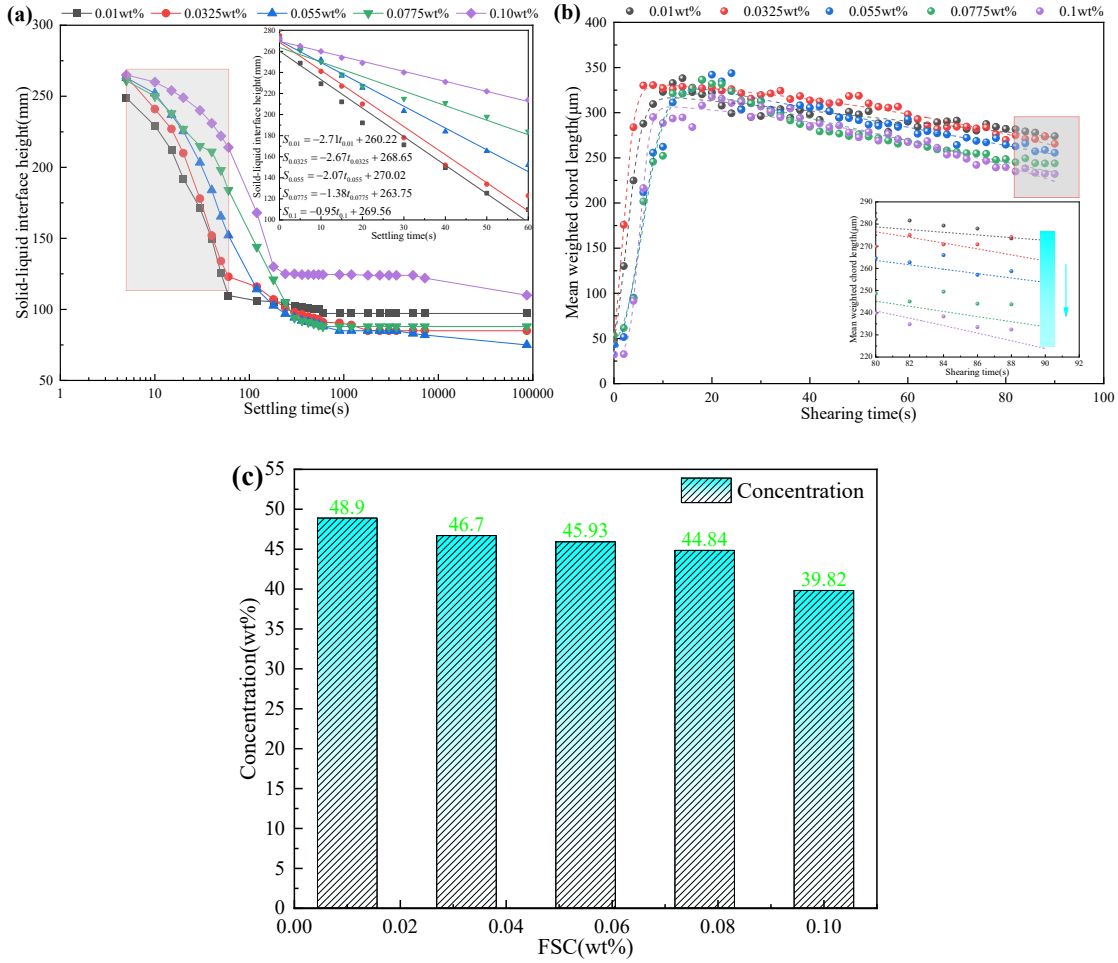

Fig. 5 Flocculation, sedimentation, and consolidation properties under different FSCs: (a) Settling curves; (b) Floc size evolution; (c) Concentration

3.1.4 Influence of SR on flocculation

The ISRs corresponding to SRs of 80, 160, 240, 320, and 400 r·min^{-1} are 1.88, 1.99, 2.18, 1.88, and 1.82 mm·s^{-1}, respectively (Fig. 6(a)). As the SR increases, the ISR first increases and then decreases, and the ISR corresponding to SR of 240 r·min^{-1} is the highest.

At a shearing time of 90 s with different SRs, the MWCLs are 102.971, 226.867, 255.612, 101.864, and 94.002 μm, respectively (Fig. 6(b)). As the SR increases, the MWCL of flocs first increases and then decreases. The floc evolution curves corresponding to different SRs conform to Asym2sig models (Table S1).

Fig. 6(c) shows that the concentrations corresponding to different SRs are 52.07, 51.66, 45.93, 41.28, and 39.64 wt%, respectively. The corresponding concentration is the highest when SR is 160 r·min^{-1}. The reasonable range of SR is 80-400 r·min^{-1}.

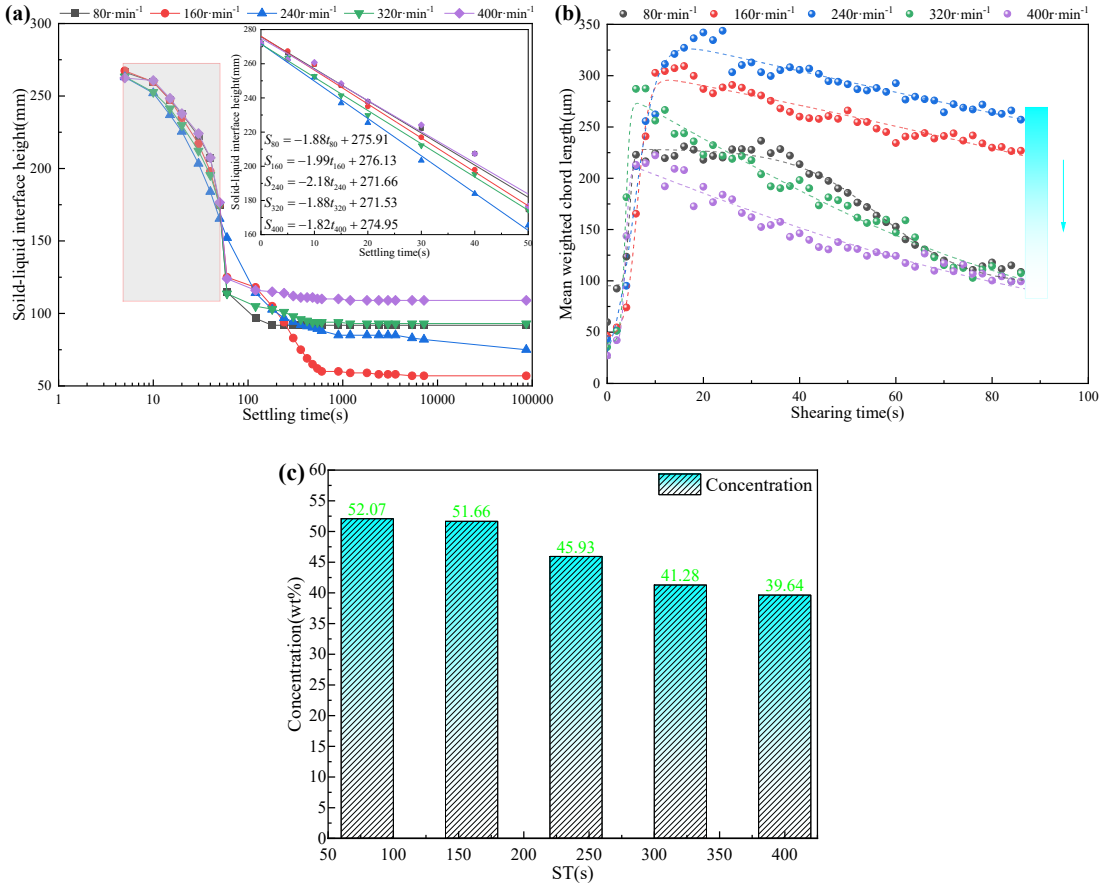

Fig. 6 Flocculation, sedimentation, and consolidation properties under different SRs: (a) Settling curves; (b) Floc size evolution; (c) Concentration

3.1.5 Influence of ST on flocculation

With the extension of ST, the settling curve moves up continuously (Fig. 7(a)). The ISRs corresponding to the different STs of 30, 60, 90, 120, and 150 s are 2.51, 2.19, 2.16, 1.91, and 1.89 mm·s^{-1}, respectively. As the ST increases, the ISR decreases continuously.

The evolution curve of MWCL moves down continuously with the increase of ST, indicating that the longer the ST, the smaller the floc size (Fig. 7(b)). The MWCLs under different shearing times are 307.448, 259.659, 255.612, 195.516, and 170.033 μm, respectively. With the prolonged ST, the MWCL decreases continuously, which also reveals the low ISR with high ST. The floc evolution curves corresponding to different STs conform to Asym2sig models (Table S1). Fig. 7(c) shows that the concentrations corresponding to different STs are 45.58, 44.35, 45.93, 44.61, and 42.05 wt%, respectively, and the concentration decreases with the continuous extension of ST. The reasonable range of ST is 30-150 s.

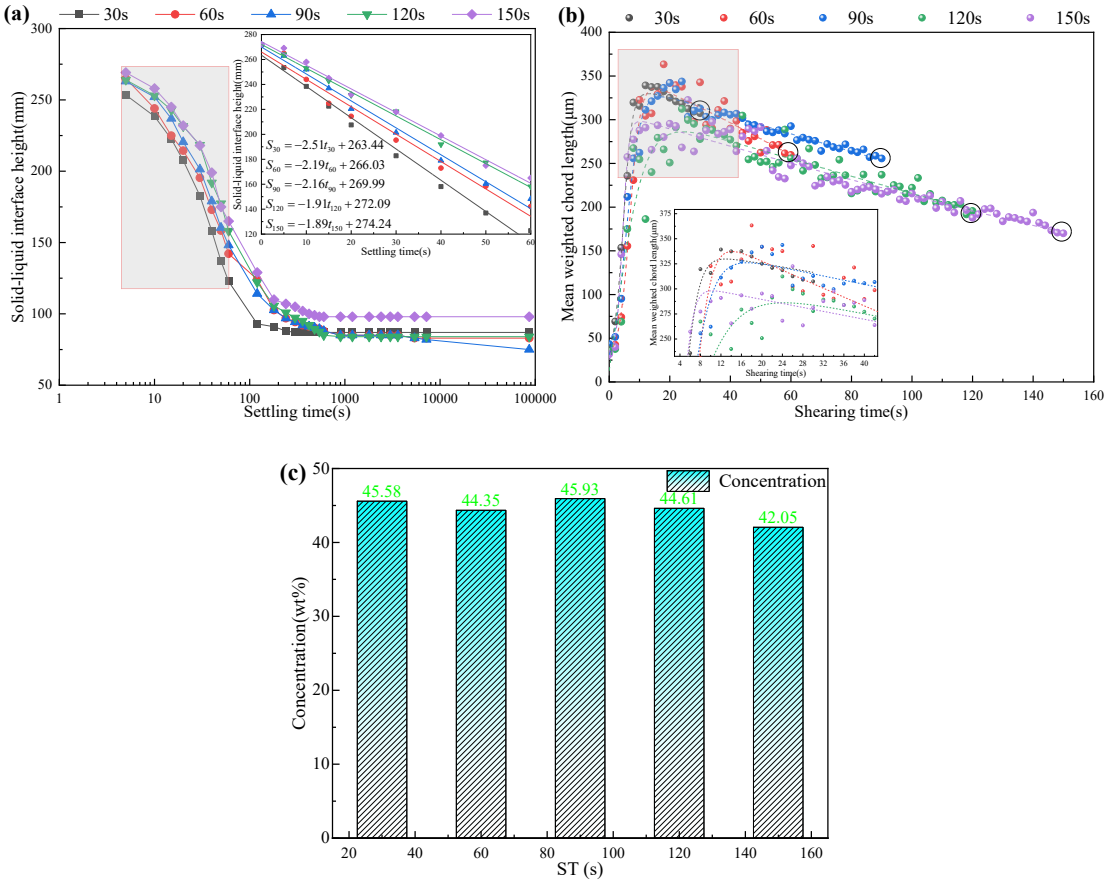

Fig. 7 Flocculation, sedimentation and consolidation properties under different STs: (a) Settling curves; (b) Floc size evolution; (c) Concentration

3.2 Flocculation mechanism based on floc evolution

3.2.1 ISR-MWCL analysis

The analysis in Section 3.1 shows a direct proportion relationship between the ISR and the MWCL under different flocculation influencing factors (TFC, FSC, SR, ST) with the APAM 645S. The larger the MWCL of flocs, the higher the ISR of tailings slurry. By fitting and analyzing the relationship between them, the fitting straight lines of ISR and MWCL are shown in Fig. 8. Therefore, ISR is a linear function of the MWCL under different flocculation conditions. The R^2 values of the fitted straight lines under the influencing factors of TFC, FSC, SR, and ST are 0.912, 0.970, 0.947, and 0.856, respectively, and the fitting effect is highly reliable, indicating that there is a strong correlation between ISR and floc size. Therefore, for tailings disposal, large-sized tailings flocs can help improve the efficiency of tailings treatment.

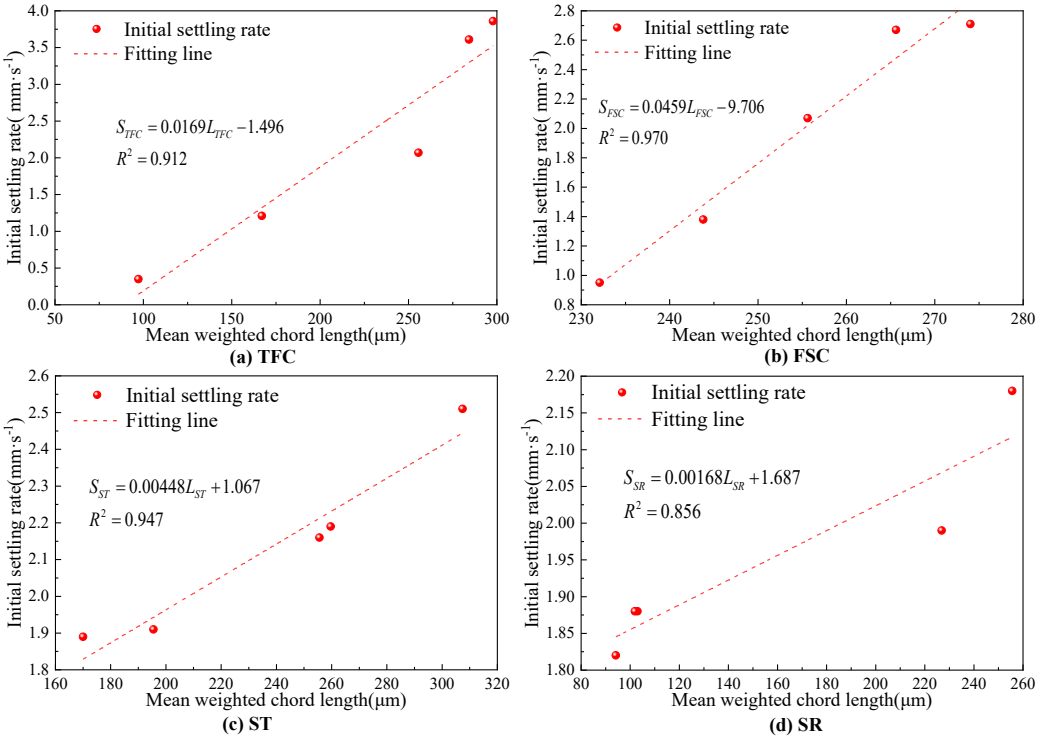

Fig. 8 ISR-MWCL correlation and characterization analysis

3.2.2 Time-dependent floc evolution mechanism

Section 3.1 shows that the floc size evolution has a time-dependent property, and its time dependence conforms to the peak function [48-49], which is suitable for Asym2sig models. The time dependence of flocs was analyzed (Fig. 9). The evolution process of flocs is mainly divided into three stages: growth stage, rupture and reconstruction stage, and stable stage.

(a) Growth stage: In the growth period, the tailings particles come into contact with the polymer chains of PAMs for the first time, and the tailings particles are adsorbed on the polymer chains, forming a large-size floc through bridging, and a large amount of free water is sealed in the flocs. During this period, flocs grow rapidly in a short time and reach the peak.

(b) Rupture and reconstruction stage: Due to continuous shearing, flocs break, and the free water sealed in flocs is released. The long polymer chains break and become shorter. Meanwhile, the shorter polymer chains are bridged to reconstruct smaller flocs, and the floc quantity increases. The rupture and reconstruction process achieves the transition of the in-floc water to the floc-floc water, making the flocs more compact.

(c) Stable stage: When the floc strength can resist the interference of the shearing effect, the flocs reach a relatively stable size. Compared with the peak size, the flocs in the stable period are smaller. The floc size in the stable period has a decisive influence on the ISR of tailings slurry. The larger the floc size, the greater its gravity and the higher its ISR.

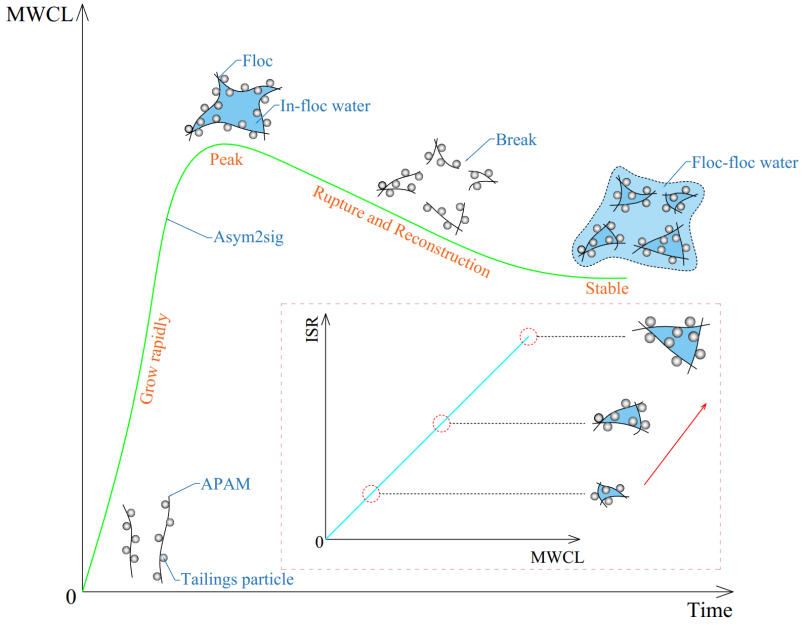

Fig. 9 Evolution mechanism of flocs size time dependence

3.3 Multi-factor optimization of flocculation based on RSM-BBD

3.3.1 RSM-BBD experimental results

The experimental results of tailings flocculation and sedimentation based on RSM-BBD are shown in Figures 10 and 11. Fig. 10 shows the solid-liquid interface curves of different experimental groups, while Fig. 11 shows the MWCL evolution curves of flocs in different experimental groups. The MWCL curves of flocs in different experimental groups meet the Asym2sig model (fitting results are in Table S2). The corresponding response values of different experimental groups, the concentration, and the MWCL at the end of shearing are shown in Table 5. Group 7 has the highest concentration (59.58 wt%), and group 22 has the largest MWCL of flocs (302.471 μm).

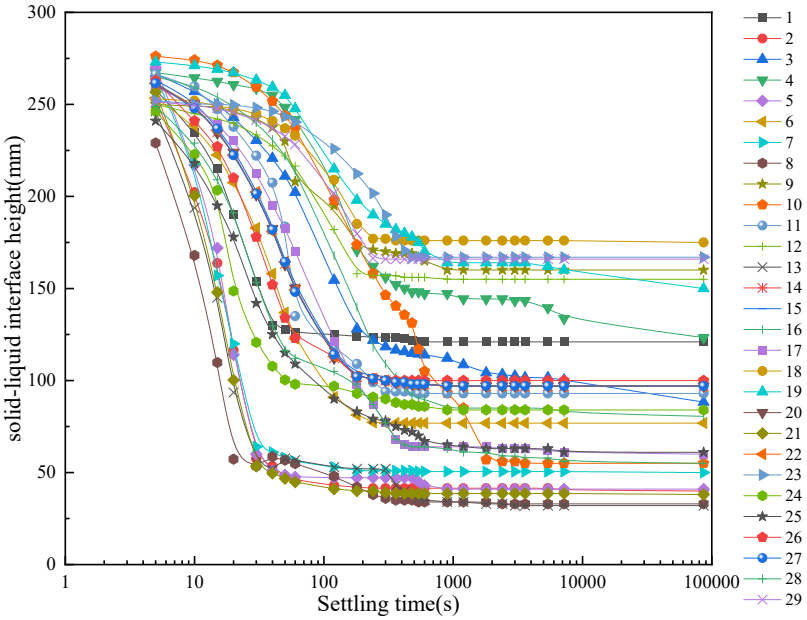

Fig. 10 Settling curves of different experimental groups based on RSM-BBD

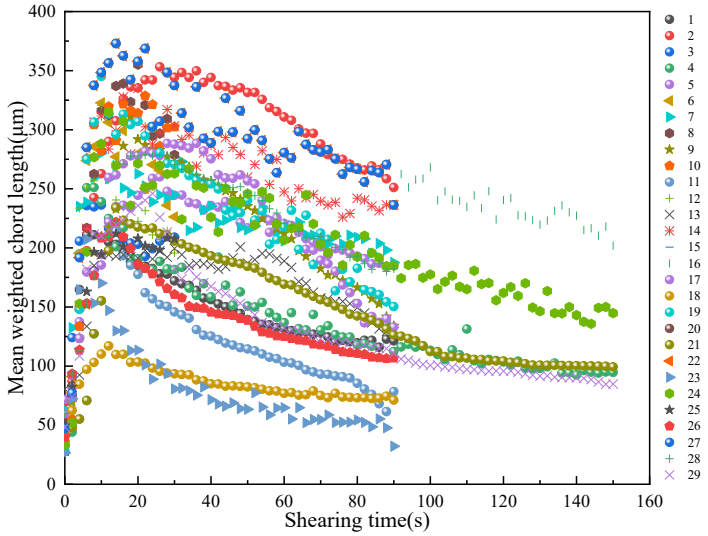

Fig. 11 MWCL evolution of different experimental groups based on RSM-BBD

Table 5 RSM-BBD experiment results

NO.	TFC (wt%)	FSC (wt‰)	SR ($r \cdot min^{-1}$)	ST (s)	Concentration (wt%)	MWCL (μm)	concentration predicted value	MWCL predicted value
1	1	0	1	0	35.825	32.123	34.58	21.013
2	0	-1	1	0	44.055	106.831	44.93	119.602
3	0	0	0	0	45.17	236.357	45.17	236.92
4	-1	0	1	0	51.149	187.602	50.933	178.191
5	0	1	1	0	43.959	121.315	43.738	145.383
6	0	1	0	1	49.485	202.028	49.488	181.767
7	-1	1	0	0	59.58	251.134	59.003	230.627
8	0	0	0	0	45.174	236.357	45.17	236.92
9	-1	-1	0	0	54.432	185.378	53.141	171.587
10	0	0	0	0	45.174	236.357	45.17	236.92
11	0	0	1	1	40.274	94.608	40.298	82.096
12	0	0	-1	1	52.853	132.971	51.634	126.448
13	1	0	-1	0	43.643	134.008	44.109	125.749
14	0	0	0	0	45.174	236.357	45.17	236.92
15	-1	0	-1	0	56.092	128.945	57.587	122.607
16	0	1	-1	0	50.048	118.342	49.366	130.791
17	-1	0	0	1	54.717	99.303	55.634	143.499
18	1	1	0	0	33.722	71.185	34.57	81.182
19	1	0	0	1	36.1826	84.825	36.768	100.681
20	0	-1	0	1	46.46	144.761	46.069	128.194
21	0	-1	-1	0	55.066	182.309	55.484	183.346
22	0	-1	0	-1	56.379	302.471	56.612	305.146
23	0	1	0	-1	45.241	226.213	45.883	224.799
24	-1	0	0	-1	55.548	278.657	55.153	287.691
25	0	0	1	-1	46.254	209.042	47.013	211.864
26	0	0	0	0	45.174	236.357	45.17	236.92
27	1	-1	0	0	47.616	150.314	47.743	166.997
28	1	0	0	-1	44.913	195.722	44.188	176.473
29	0	0	-1	-1	52.336	207.708	51.859	216.664

3.3.2 Multiple nonlinear regression model

The experimental data in Table 5 was analyzed using Design Expert software. Through regression analysis, multiple nonlinear regression models were established with concentration and test-ending MWCL as dependent variables (Equation (2)).

$$Y = \beta_0 + \sum_{i=1}^{n} \beta_i x_i + \sum_{i=1}^{n} \beta_{ii} x_i^2 + \sum_{i<j} \beta_{ij} x_i x_j \quad (2)$$

Where Y is the response value; β_0 is the constant term; β_i is the coefficient of the first-order term; β_{ii} is the coefficient of the quadratic term; β_{ij} is the interaction term coefficient; n is the number of experimental factors. In this experiment, n = 4; x_i, x_j are the coded values of experimental factors.

$$\begin{aligned} Y_1 = {} & 0.0166x_1^2 + 0.124x_2^2 + 0.0000273x_3^2 + 0.000509x_4^2 - 0.141x_1x_2 \\ & -0.000599x_1x_3 - 0.00439x_1x_4 + 0.00171x_2x_3 + 0.0131x_2x_4 \\ & -0.000169x_3x_4 - 0.261x_1 - 0.892x_2 - 0.0221x_3 - 0.0752x_4 + 70.095 \end{aligned} \quad (3)$$

$$\begin{aligned} Y_2 = {} & -0.953x_1^2 - 1.023x_2^2 - 0.00279x_3^2 - 0.00173x_4^2 \\ & -1.073x_1x_2 - 0.0334x_1x_3 + 0.0380x_1x_4 + 0.0272x_2x_3 + 0.124x_2x_4 \\ & -0.00103x_3x_4 + 38.718x_1 + 10.855x_2 + 1.790x_3 - 1.705x_4 - 170.308 \end{aligned} \quad (4)$$

Where Y_1 is concentration, wt%; Y_2 is the mean weighted chord length of flocs, μm; x_1 is the tailings feeding concentration, wt%; x_2 is the flocculant solution concentration, wt‰; x_3 is the shear rate, r·min^{-1}; x_4 is the shear time, s.

The predictive ability of the regression equation models mentioned above was verified by comparing the predicted values of the regression models (Eq. (3) and (4)) with the experimental values. The experimental values of concentration and MWCL were taken as the X-axis, and the predicted values of the models were taken as the Y-axis for analysis. Additionally, the Y=X line was used for fitting. Fig. 12(a) shows the error analysis of the concentration response model. The data points are closely distributed on both sides of the 1:1 line, the dispersion of the predicted value is small, and the error of the data points is less than 4%. Fig. 12(b) shows the error analysis of the MWCL response model. The error between the predicted value and the experimental value with the MWCL in the range of 100-150 μm is large. The other predicted values are closely distributed on both sides of the 1:1 line, and the error of the predicted value is less than 20%. This indicates that the regression models with concentration and MWCL as response values have good predictive ability.

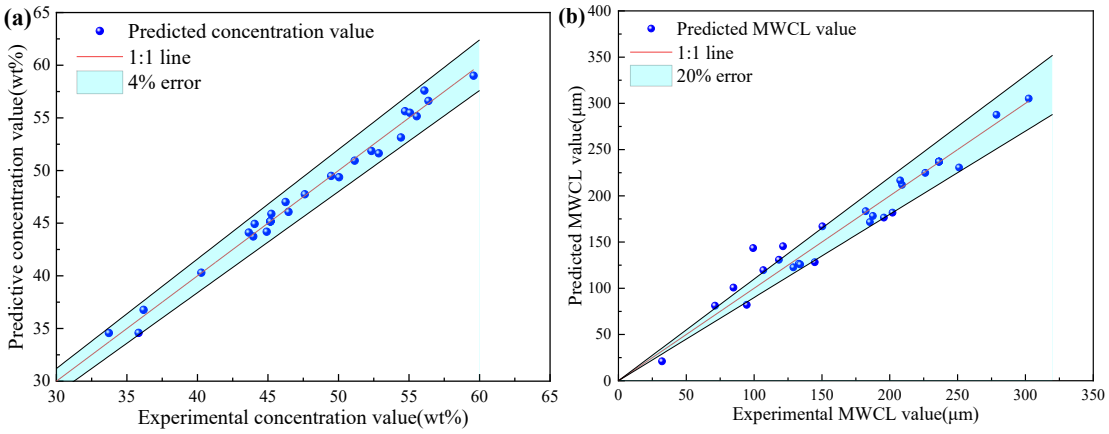

Fig. 12 Reliability analysis of regression models: (a) Concentration model; (b) MWCL model

3.3.3 Variance analysis

The variance analysis of Eq. (3) and (4) is shown in Table 6. The *F* values of the equations with the concentration and the MWCL as the response values are 14.44 and 27.20, respectively, which are both greater than $F_{0.01}(5.03)$, and the *p* values are both less than 0.0001, indicating that the above regression equations are significant. The R^2 of the regression equation with the concentration and the MWCL as the response values are 0.9890 and 0.9541, respectively, and the R^2_{adj} are 0.9780 and 0.9083, respectively, which shows that the factors of the regression models have a strong correlation with the response values and also proves that the regression models are extremely reliable.

Table 6 Variance analysis of concentration and MWCL models

Response value	*F* value	*P* value	R^2	R^2_{adj}
Concentration	14.44	<0.0001	0.9890	0.9780
MWCL	27.20	<0.0001	0.9541	0.9083

Table 7 shows the variance analysis of each item in the regression equation of concentration and MWCL. Among them, in the variance analysis of the concentration regression equation, the *F* values of each term are basically greater than $F_{0.01}(5.03)$, and the *P* values of x_1, x_2, x_3, x_1x_2, x_2x_4, x_2^2, and the misfitting term are all less than 0.0001, which shows that the statistical significance is extremely strong. The *F* value of the first-order term indicates the degree of influence of flocculation factors on the concentration, and the order of influence degree is: x_1 (TFC) > x_3 (SR) > x_2 (FSC) > x_4 (ST), which shows that TFC has the most significant influence on the concentration. The order of the interaction terms, that is, the interaction between the influencing factors on the concentration is as follows: x_1x_2 (TFC-FSC) > x_2x_4 (FSC-ST) > x_1x_4 (TFC-ST) > x_3x_4 (SR-ST). In the variance analysis of the regression equation for the MWCL, *F* values of most terms are greater than $F_{0.01}(5.03)$, and *P* values of x_3, x_4, x_1^2, and x_3^2 are less than 0.0001. The order of influence degree of each influencing factor represented by the first term of *F* values on the MWCL is as follows: x_4 (ST) > x_3 (SR) > x_1 (TFC) > x_2 (FSC), indicating that ST has the most significant effect on the MWCL, which also verifies that the evolution of floc size is time-dependent. The influence degree of the interaction factors

represented by the interaction terms in *F* value on the MWCL is ranked as: x_1x_3 (TFC-SR)> x_1x_2 (TFC-FSC)> x_2x_4 (FSC-ST).

Table 7 Variance analysis of each item in the concentration and MWCL regression models

Source	Adj SS		Adj MS		F		P	
	Y_1	Y_2	Y_1	Y_2	Y_1	Y_2	Y_1	Y_8
Model	1170.12	12138 6	83.58	8670.43	89.95	20.81	< 0.0001	< 0.0001
x_1	346.51	2347.47	346.51	2347.47	372.91	5.63	< 0.0001	0.0325
x_2	41.03	1895.7	41.03	1895.7	44.16	4.55	< 0.0001	0.0511
x_3	94.65	14556. 47	94.65	14556. 47	101.86	34.93	< 0.0001	< 0.0001
x_4	5.72	17244. 24	5.72	17244. 24	6.15	41.38	0.0265	< 0.0001
x_1x_2	90.65	5247.92	90.65	5247.92	97.56	12.59	< 0.0001	0.0032
x_1x_3	2.07	6443.43	2.07	6443.43	2.22	15.46	0.1582	0.0015
x_1x_4	15.6	1171.59	15.6	1171.59	16.79	2.81	0.0011	0.1158
x_2x_3	6.06	1538.64	6.06	1538.64	6.52	3.69	0.023	0.0753
x_2x_4	50.15	4457.23	50.15	4457.23	53.97	10.7	< 0.0001	0.0056
x_3x_4	10.55	393.96	10.55	393.96	11.35	0.95	0.0046	0.3474
x_1^2	5.62	18638. 05	5.62	18638. 05	6.05	44.72	0.0275	< 0.0001
x_2^2	40.84	2784.28	40.84	2784.28	43.95	6.68	< 0.0001	0.0216
x_3^2	3.16	33186. 32	3.16	33186. 32	3.4	79.63	0.0865	< 0.0001
x_4^2	21.82	250.52	21.82	250.52	23.48	0.6	0.0003	0.451
Residual	13.01	5834.23	0.93	416.73				
Misfitting term	13.01	5834.23	1.3	583.42	4552 23		< 0.0001	
Net error	1.14E-05	0	2.86E-06	0				

3.3.4 Interaction analysis

(1) Interaction analysis of concentration

The interaction between the flocculation factors on the concentration is shown in Fig. 13. To eliminate the influence of factors other than interaction factors, the other two factors are taken as the middle value in the interaction analysis. The contours of each subgraph show different degrees of curvature, indicating that the interaction of the two factors has a significant effect on the concentration. The following is a detailed analysis of the interaction on the concentration.

Fig. 13(a) shows the interaction between TFC and FSC on the concentration, exhibiting a large curvature, and the interaction between the two factors is relatively significant. When TFC is 10-11 wt% and FSC is 8-10 wt‰, the concentration reached the maximum of 59.10 wt%. When FSC drops to 8-10

wt‰, TFC increases while the concentration decreases. When TFC is greater than 24 wt%, the higher the FSC, the lower the concentration.

Fig. 13(b) shows the interaction between TFC and SR on the concentration, which generally exhibits a small curvature, mostly in a straight line, and the interaction between the two factors is not significant. When TFC is 10-12 wt% and SR is 80-160 r·min^{-1}, the maximum concentration can reach 57.60 wt%.

Fig. 13(c) shows the interaction between TFC and ST on concentration, which generally exhibits a small curvature, and there is a weak interaction between the two factors. When TFC is 10-11.5 wt% and ST is 30-150 s, the maximum concentration of 55.65 wt% can be obtained.

Fig. 13(d) shows the interaction between FSC and SR on concentration, exhibiting a large curvature overall, and the interaction between them is obvious. When FSC is 1-2 wt‰ and SR is 80-100 r·min^{-1}, the maximum concentration can be 55.50 wt%. When FSC is 1-2 wt‰ or 6-10 wt‰, the higher the SR, the lower the concentration.

Fig. 13(e) shows the interaction between FSC and ST on concentration, exhibiting a large curvature overall, and the interaction between the two factors is remarkable. When FSC is 1-1.5 wt‰ and ST is 30-37 s, the maximum concentration can reach 56.65 wt%. When FSC is 1-1.5 wt‰, the longer the ST, the lower the concentration.

Fig. 13(f) shows the interaction between SR and ST on concentration, which shows a certain curvature distribution, and the interaction between the two factors is more obvious. When SR is 80-130 r·min^{-1} and ST is 30-150 s, the maximum concentration can be 51.90 wt%. When ST is 110-160 s, the higher the SR, the lower the concentration. When SR is 360-400 r·min^{-1}, the concentration decreases with the extension of ST.

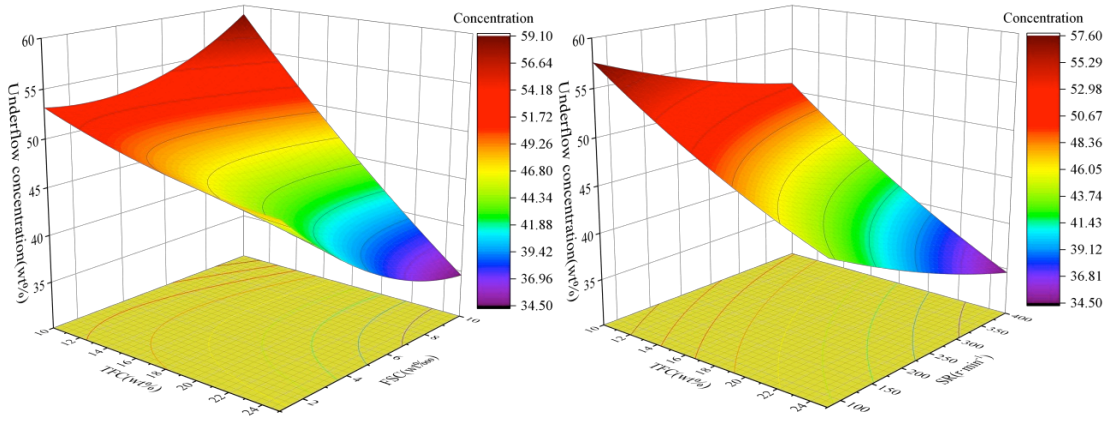

(a) TFC-FSC (b)TFC-SR

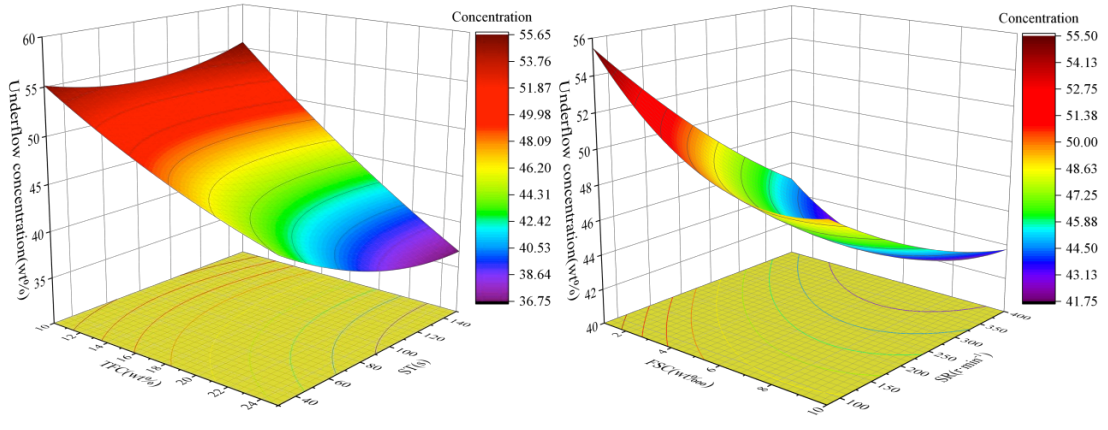

(c) TFC-ST (d)FSC-SR

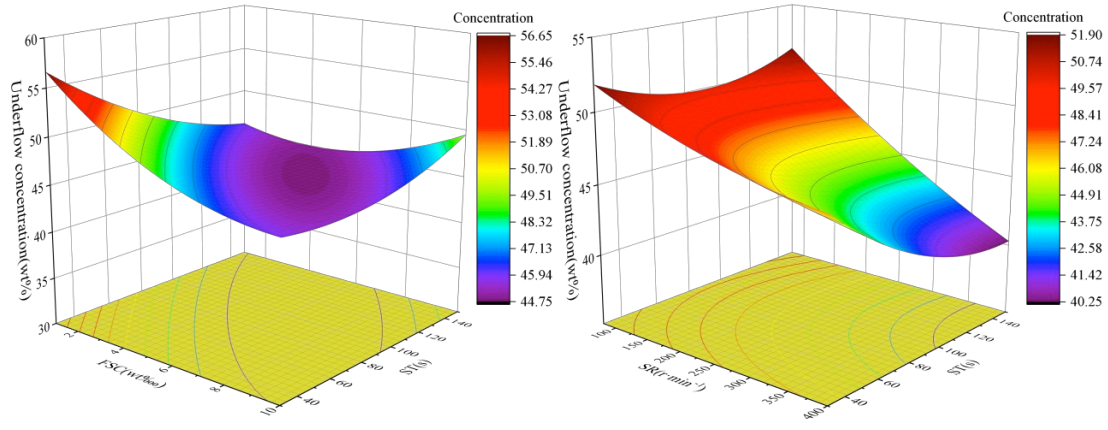

(e) FSC-ST (f)SR-ST

Fig. 13 Analysis of the interaction on concentration

(b) Interaction analysis of MWCL

The interaction of flocculation factors on the MWCL of flocs is shown in Fig. 14. Fig. 14(a) shows the interaction between TFC and FSC on the MWCL, showing great curvature in general, and the interaction between the two factors is extremely significant. When TFC is 10-19 wt% and FSC is 1.5-10 wt‰, the MWCL can reach the maximum value of 245 μm. When FSC is less than 6.8 wt‰, with the increase of TFC, the MWCL first increases and then decreases. Fig. 14(b) shows the interaction between TFC and SR on the MWCL, and the contour line in the figure is basically oval, indicating that the interaction between the two factors is extremely significant. When TFC is 10-19.5% and SR is 150-340 r·min^{-1}, the maximum MWCL is 244 μm. When TFC is 10-19.5 wt%, with the increase of SR, the MWCL first increases and then decreases.

Fig. 14(c) shows the interaction between TFC and ST on the MWCL, which generally shows a large curvature, indicating a strong interaction between the two factors. When TFC is 10-17.5 wt% and ST is 30-48 s, the MWCL can reach the maximum value of 300.5 μm. When TFC is less than 17.5 wt%, the MWCL decreases with the extension of ST. As ST increases from 30-150 s, with the increasing of TFC, the MWCL first increases and then decreases.

Fig. 14(d) shows the interaction between FSC and SR on the MWCL. The

contour curvature in the figure is obvious, and the interaction between the two factors is significant. When FSC is 1-8 wt‰ and SR is 150-280 r·min^{-1}, the MWCL can reach the maximum value of 238.5 μm. When FSC is 1-10 wt‰, with the continuous increase of SR, the MWCL first increases and then decreases.

The interaction between FSC and ST shown in Fig. 14(e) has a small volume curvature, and the interaction between the two factors is weak. When FSC is 1-5 wt‰ and ST is 30-48 s, the MWCL can reach the maximum value of 305.5 μm. When FSC is 1-2.2 wt‰, the MWCL decreases with the continuous extension of ST. When ST is less than 48 s or more than 130 s, the MWCL decreases with the increasing FSC.

Fig. 14(f) shows that the interaction between SR and ST has a great curvature on the MWCL, and the interaction between the two factors is remarkable. When SR is 150-325 r·min^{-1} and ST is 30-56.7 s, the MWCL can reach the maximum value of 286 μm. When SR is 80-400 r·min^{-1}, the MWCL decreases with the continuous extension of ST. When ST is 30-150 s, the MWCL first increases and then decreases with the continuous increase of ST.

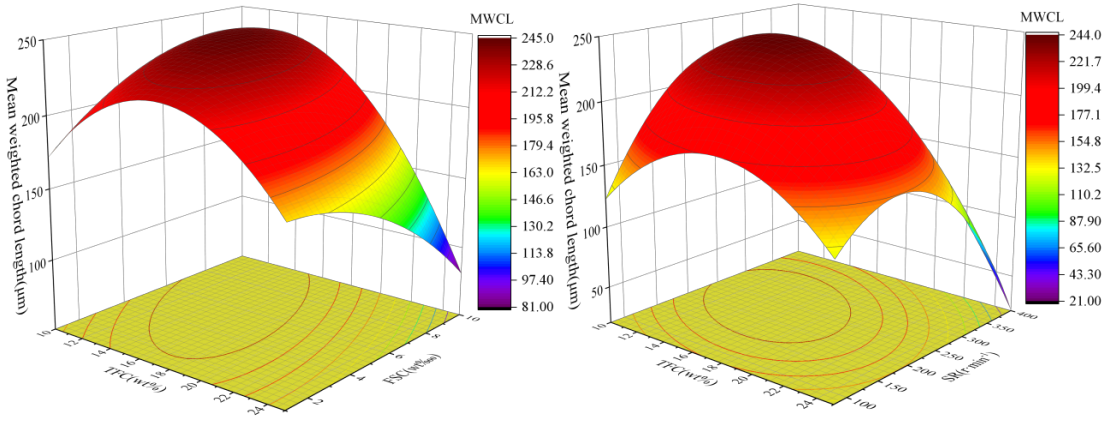

(a) TFC-FSC

(b)TFC-SR

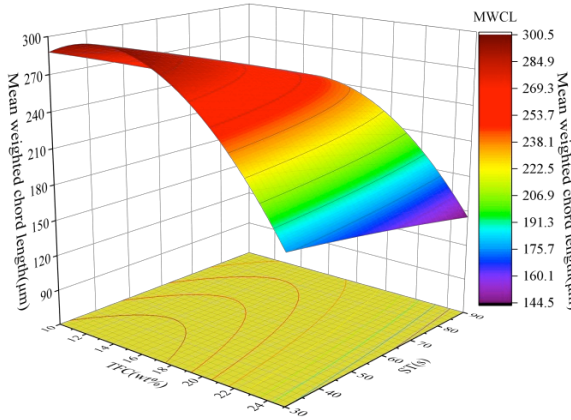

(c) TFC-ST

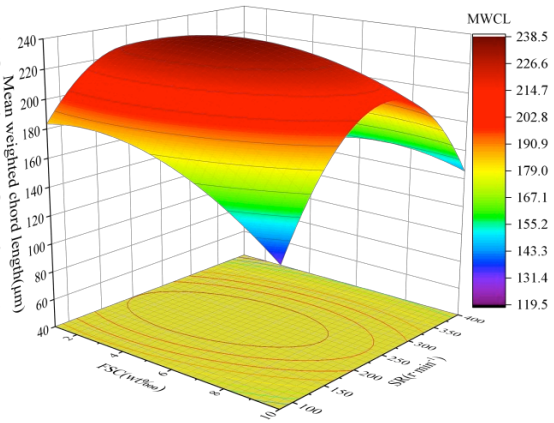

(d)FSC-SR

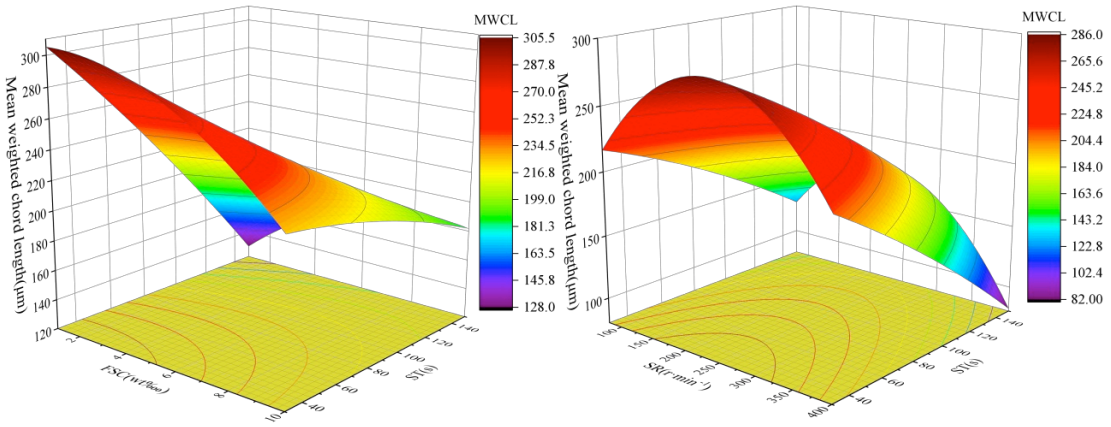

(e) FSC-ST (f)SR-ST

Fig. 14 Analysis of the interaction on MWCL

3.3.5 Optimization results based on RSM-BBD

By using the optimization function in Design Expert software, the flocculation conditions can be optimized. The ultimate goal of thickening is to obtain a higher concentration and higher tailings processing efficiency. The processing efficiency has a great relationship with the ISR of flocs. The larger the floc size, the faster the ISR, and the higher the processing efficiency [13-14]. Therefore, the optimization of flocculation conditions based on RSM-BBD aims to obtain the highest concentration and the MWCL, and finally, obtain the optimal flocculation conditions. Among them, TFC is 17.05 wt%, FSC is 1.00 wt‰, SR is 166.11 r·min^{-1}, and ST is 30 s. Under the optimal flocculation conditions, the theoretical response values of concentration and MWCL are 58.48 wt% and 299.694 μm, respectively.

3.4 Multi-objective optimization based on RSM-BBD-DF

3.4.1 Optimization results based on RSM-BBD-DF

To obtain a more reliable optimal value of flocculation conditions, a nonlinear multi-objective optimization algorithm with Desirability Function (DF) is introduced to optimize flocculation conditions. The optimization process of flocculation conditions based on RSM-BBD-DF is shown in Fig. 15. Firstly, the MWCL and concentration in different experimental groups were obtained by carrying out flocculation and sedimentation experiments with four factors (TFC, FSC, SR, and ST) of RSM-BBD. Then, a multivariate nonlinear regression model was established with MWCL and concentration as response values, respectively. According to the multivariate nonlinear regression model, the single-DF values are calculated by Eq. (5), in which Eq. (5a) is applicable to the response variable with a higher DF value as the response value is larger. Eq. (5b) is applicable to the response variable with a higher DF value as the response value is smaller. Eq. (5c) is applicable to the response variable with the optimal target value set, and the DF value with the target value closest to the setting is greater. Based on the single-DF value of each response value, the weighted geometric average multi-objective optimization function of each

single-DF value is calculated according to the overall-DF equation shown in Eq. (6), thus the overall-DF values are obtained.

$$d_i(Y_i)=\begin{cases}0 & (Y_i<L_i)\\ \dfrac{Y_i-L_i}{U_i-L_i} & (L_i\le Y_i\le U_i)\\ 1 & (Y_i>U_i)\end{cases}\qquad \text{(a)}$$

$$d_i(Y_i)=\begin{cases}0 & (Y_i<U_i)\\ \dfrac{Y_i-U_i}{L_i-U_i} & (L_i\le Y_i\le U_i)\\ 1 & (Y_i>L_i)\end{cases}\qquad \text{(b)}$$

$$d_i(Y_i)=\begin{cases}0 & (Y_i\le L_i)\\ \dfrac{Y_i-L_i}{G_i-L_i} & (L_i\le Y_i<G_i)\\ 1 & (Y_i=G_i)\\ \dfrac{U_i-Y_i}{U_i-G_i} & (G_i<Y_i\le U_i)\\ 0 & (Y_i>U_i)\end{cases}\qquad \text{(c)}$$

(5)

Where d_i is the DF of the *i*-th response value; Y_i is the *i*-th response value; L_i, U_i and G_i are the lower limit, upper limit and optimal target value of the *i*-th response value, respectively.

$$D=\left(\prod_{i=1}^{s}d_i^{e_i}\right)^{\frac{1}{\sum e_i}} \qquad (6)$$

s and e_i are the number and weight of the response value, respectively, and the weight indicates the importance of the response value.

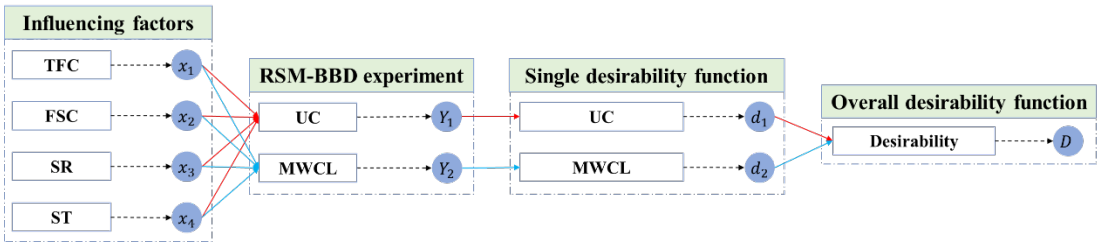

Fig. 15 Optimization process of flocculation conditions based on RSM-BBD-DF

Both the concentration and the MWCL of flocs are equally important to the thickening effect, so it is considered that the weights of concentration and the MWCL are 0.5, respectively, that is, e_1=e_2=5. Because both the concentration and the MWCL are at their maximum, the single DF of Eq. (5a) is used to calculate, and finally, the overall-DF values of different flocculation factors are obtained as shown in Fig. 16(a). The ST has the greatest influence on the overall-DF value of the thickening effect. With the continuous extension of the ST, the overall-DF values decrease, and the highest overall-DF value (0.612) is achieved when ST is 30 s. When TFC is 10-18 wt%, the overall-DF values first increase and then decrease. The FSC has little effect on the overall-DF value

of the thickening effect and has the highest overall-DF value with 1-3 wt‰. With the increase of SR, the overall-DF values first increase and then decrease, with the highest overall-DF value of 160-200 r·min^{-1}.

Based on the optimal values and ranges of the above flocculation factors, optimize the flocculation conditions. Taking TFC as a variable, the FSC is 1, 2, and 3 wt‰, the SR is 160, 180, and 200 r·min^{-1}, and ST is 30 s. The influence of multiple factors on the overall-DF values of the thickening effect is shown in Fig. 16(b), and it is found that the highest overall-DF value (0.956) is achieved when TFC is 17 wt%, the FSC is 1 wt‰, the SR is 160 r·min^{-1} and ST is 30 s. This is basically consistent with the multi-objective optimization results of Design Expert software. Therefore, the optimal flocculation conditions are determined as follows: TFC is 17 wt%, the FSC is 1wt‰, the SR is 160 r·min^{-1}, and ST is 30 s.

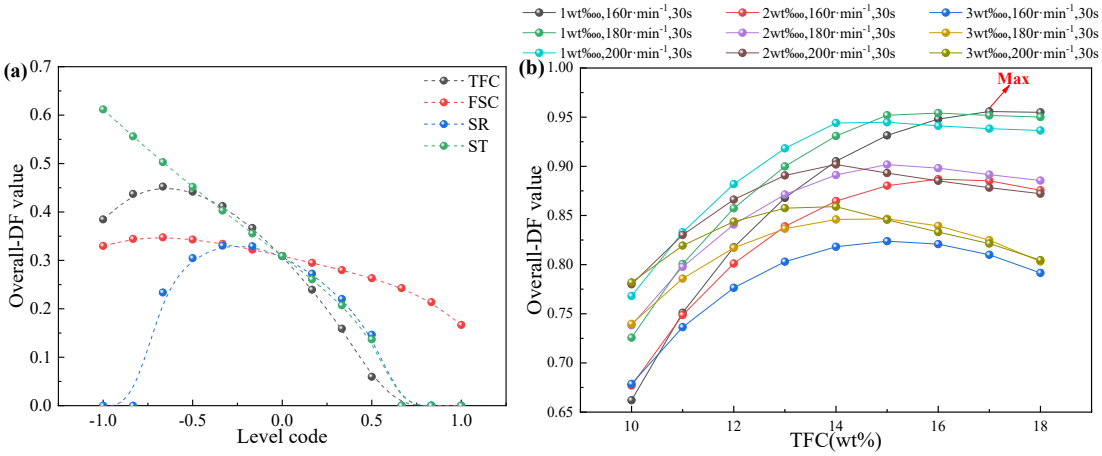

Fig. 16 Optimization results of flocculation conditions based on RSM-BBD-DF: (a) Single factor; (b) Multiple factors

3.4.2 Optimization results verification

The optimal flocculation conditions obtained above were verified. The optimal flocculation conditions obtained by Design Expert software (TFC: 17.05 wt%, FSC: 1 wt‰, SR: 166 r·min^{-1}; ST: 30 s) and RSM-BBD-DF multi-objective method (TFC: 17 wt%, FSC: 1 wt‰, SR: 160 r·min^{-1}; ST: 30 s) were experimentally verified using the experimental device shown in Fig. 2. The obtained concentration and MWCL are shown in Table 8. It can be seen from Table 8 that the experimental values under the optimal flocculation conditions obtained by the Design Expert are basically consistent with the predicted values, and the error is 0.91% and 2.34%. The concentration and the MWCL under the optimal flocculation conditions obtained by RSM-BBD-DF are not much different from those obtained by the Design Expert. It shows that the multi-objective optimization method based on RSM-BBD-DF has high reliability for flocculation conditions optimization.

Table 8 Validation of optimization results

	Predicted value	Design Expert experimental value	RSM-BBD-DF experimental value
Concentration(wt%)	58.48	57.95	58.92
MWCL(μm)	299.694	292.658	302.279

4 Conclusion

In this study, the time dependence of floc size and the relationship between ISR and MWCL were quantitatively characterized by testing floc size and concentration under different influencing factors. Through experiments based on RSM-BBD, correlation regression models were established, and the interaction of various flocculation conditions was analyzed. Finally, the optimal flocculation conditions were obtained and verified based on the RSM-BBD-DF. The conclusions can be drawn as follows:

(1) The evolution of floc size is time-dependent, and its evolution with shearing time accords with the Asym2sig model, which shows that floc first grows rapidly and then slowly decreases until it is stable. Floc has experienced growth, rupture, and reconstruction, and a stable period.

(2) There is a linear relationship between ISR and the test-ending MWCL, that is, the larger the floc size, the higher the ISR, and the mechanism of floc structure evolution is revealed from the perspective of the interaction between tailings particle and APAM polymer chains.

(3) Through variance analysis of the regression models of RSM-BBD, it is found that TFC has the highest influence on the concentration. ST has the greatest influence on the MWCL, indicating a strong time-dependent evolution of floc size.

(4) The interaction between the influencing factors shows that the interaction between TFC and FSC has the highest influence on the concentration. The interaction between TFC and SR has the highest influence on the MWCL of flocs.

(5) Based on the multi-objective optimization method of RSM-BBD-DF, the optimal flocculation conditions are as follows: TFC is 17 wt%, FSC is 1 wt‰, SR is 160 $r \cdot min^{-1}$, and ST is 30 s. Under these optimal flocculation conditions, the concentration is 58.92 wt%, and the MWCL of flocs is 302.279 μm.

Acknowledgment

This work was funded by the National Natural Science Foundation of China (no. 52130404, 52304121), the Fundamental Research Funds for the Central Universities (no.FRF-TP-22-112A1), Guangdong Basic and Applied Basic Research Foundation (no. 2021A1515110161), ANID (Chile) through Fondecyt project 1210610, Centro de Modelamiento Matemático (BASAL funds for Centers of Excellence FB210005), CRHIAM project ANID/FONDAP/15130015 and ANID/FONDAP/1523A0001, and Anillo project ANID/ACT210030.

Declaration of Interest Statement

The authors declare no conflict of interest.

References

[1] Y. Wang, Z.Q. Wang, A.X. Wu, Wang L, Q. Na, C. Cao, G.F. Yang, Experimental research and numerical simulation of the multi-field performance of cemented paste backfill: Review and future perspectives, *INT. J. MIN. MET. MATER.*, 2023, 30(2):193-208.

[2] S.H. Yin, Y.J. Shao, A.X. Wu, H.J. Wang, X.H. Liu, Y. Wang, A systematic

review of paste technology in metal mines for cleaner production in China, *J. CLEAN. PROD.*, 2020, 247.

[3] C.C. Qi, A. Fourie, Cemented paste backfill for mineral tailings management: Review and future perspectives, *MINER. ENG.*, 2019, 144.

[4] S.K. Behera, D.P. Mishra, P. Singh, K. Mishra, S.K. Mandal, C.N. Ghosh, R. Kumar, P.K. Mandal, Utilization of mill tailings, fly ash and slag as mine paste backfill material: Review and future perspective, *CONSTR. BUILD. MATER.*, 2021, 309.

[5] A. Tariq, E.K. Yanful, A review of binders used in cemented paste tailings for underground and surface disposal practices, *J. ENVIRON. MANAG.*, 2013, 131: 138-149.

[6] C.C. Vargas, A.M. Pulido, Sustainable Management of Thickened Tailings in Chile and Peru: A Review of Practical Experience and Socio-Environmental Acceptance, *SUSTAINABILITY.*, 2022, 14(17).

[7] A.X. Wu, Z.E. Ruan, J.D. Wang, Rheological behavior of paste in metal mines, *INT. J. MIN. MET. MATER.*, 2022, 29: 717–726.

[8] D. Liu, M. Edraki, P. Fawell, L. Berry, Improved water recovery: A review of clay-rich tailings and saline water interactions, *POWDER. TECHNOL.*, 2020, 364: 604-621.

[9] V. Vajihinejad, S.P. Gumfekar, B. Bazoubandi, Z.R. Najafabadi, J.B.P. Soares, Water Soluble Polymer Flocculants: Synthesis, Characterization, and Performance Assessment, *MACROMOL. MATER. ENG.*, 2019.

[10] K. Asgari, H. Khoshdast, F. Nakhaei, M.R. Garmsiri, Q.Q. Huang, A. Hassanzadeh, A Review on Floc-Flotation of Fine Particles: Technological Aspects, Mechanisms, and Future Perspectives, *MINER. PROCESS. EXTR. M.*, 2023.

[11] A.A. Moud. Polymer based flocculants: Review of water purification applications. *J. WATER. PROCESS. ENG.*, 2022, 48.

[12] D. Nanda, N. R. Mandre, Mechanism of polymeric adsorption in selective flocculation of low-grade iron ore, *SEP. PURIF. TECHNOL.*, 2021, 56(1): 68-77.

[13] Y. Li, D.V. Zyl, Hindered settling of flocculated multi-sized particle suspension, part I: Segregation mechanism of non-flocculated particles, *POWDER. TECHNOL.*, 2022, 407.

[14] E. Sabah, I. Cengiz, An evaluation procedure for flocculation of coal preparation plant tailings, *WATER. RES.*, 2004, 38(6): 1542-1549.

[15] A.X. Wu, Z.E. Ruan, R. Bürger, S.H. Yin, J.D. Wang, Y. Wang, Optimization of flocculation and settling parameters of tailings slurry by response surface methodology, *MINER. ENG.*, 2020,156.

[16] H.Z. Jiao, Y.C. Wu, H. Wang, X.M. Chen, Z. Li, Y.F. Wang, B.Y. Zhang, J.H. Liu, Micro-scale mechanism of sealed water seepage and thickening from tailings bed in rake shearing thickener, *MINER. ENG.*, 2021,173.

[17] G.Z. Chen, C.P. Li, Z.E. Ruan, R. Bürger, H.Z. Hou, Research on floc

709 structure and physical properties based on pipeline flocculation, *J. WATER. PROCESS. ENG.*, 2023, 53
711 [18] S.C. Chen, M.Y. Gao, W.T. Lin, J.F. Liang, D.W. Li, Effects of incorporating large quantities of copper tailings with various particle sizes on the strength and pore structure of cement-based materials, CONSTR. BUILD. MATER., 2022, 329
715 [19] Y.Y. Tan, X. Meng, Z.W. Jiang, C.C. Han, M.C. Guo, Research on Flocculant Selection for Classified Fine Tailings Based on Micro-Characterization of Floc Structure Characteristics, *MATERIALS.*, 2022, 15(7).
718 [20] J. Csavina, M.P. Taylor, O. Félix, K.P. Rine, A.E. Sáez, E.A. Betterton, Size-resolved dust and aerosol contaminants associated with copper and lead smelting emissions: Implications for emission management and human health, *SCI. TOTAL. ENVIRON.*, 2014, 493: 750-756,
722 [21] H.Z. Jiao, S.F. Wang, Y.X. Yang, X.M. Chen, Water recovery improvement by shearing of gravity-thickened tailings for cemented paste backfill, *J. CLEAN. PROD.*, 2020, 245.
725 [22] Z.J. Zhang, H.T. Nong, Y.N. Li, L. Zhao, H. Gao, Effects of ballasting particles on settling rate of iron ore tailings, *PARTICUL. SCI. TECHNOL.*, 2020, 38(4): 427-432.
728 [23] L.F. Zhang, A.X. Wu, H.J. Wang, L.M. Wang, Representation of batch settling via fitting a logistic function, *MINER. ENG.*, 2018,128: 160-167.
730 [24] R.K. Dwari, S.I. Angadi, S.K. Tripathy, Studies on flocculation characteristics of chromite's ore process tailing: Effect of flocculants ionicity and molecular mass, *COLLOID. SURFACE. A.*, 2018, 537: 467-477.
733 [25] A. Vahedi, B. Gorczyca, Application of fractal dimensions to study the structure of flocs formed in lime softening process, *WATER. RES.*, 2011, 45(2): 545-556
736 [26] S. Farrokhpay, L. Filippov, Aggregation of nickel laterite ore particles using polyacrylamide homo and copolymers with different charge densities, *POWDER. TECHNOL.*, 2017, 318: 206-213
739 [27] P. Ofori, A.V. Nguyen, B. Firth, C. McNally, O. Ozdemir. Shear-induced floc structure changes for enhanced dewatering of coal preparation plant tailings, *CHEM. ENG. J.*, 2011, 172(2-3): 914-923
742 [28] A. Govedarica, E.J.M. Bacca, M. Trifkovic, Structural investigation of tailings flocculation and consolidation via quantitative 3D dual fluorescence/reflectance confocal microscopy, *J. COLLOID. INTERF. SCI.*, 2020, 571: 194-20.
746 [29] M.R. MacIver, M. Pawlik, A floc structure perspective on sediment consolidation in thickened tailings, *CHEM. ENG. SCI.*, 2022, 263.
748 [30] W.H. Leiva, P.D. Fawell, C. Goñi, N. Toro, R.I. Jeldres, Temporal evolution of the structure of tailings aggregates flocculated in seawater, *MINER. ENG.*, 2021, 160.
751 [31] M.A. Inam, R. Khan, I.T. Yeom, A.S. Buller, M. Akram, M.W. Inam,

752 Optimization of Antimony Removal by Coagulation-Flocculation-
753 Sedimentation Process Using Response Surface Methodology,
754 *PROCESSES.*, 2021, 9(1).
755 [32] D.J. Venegas-García, L.D. Wilson, Utilization of Bioflocculants from
756 Flaxseed Gum and Fenugreek Gum for the Removal of Arsenicals from
757 Water, *MATERIALS.*, 2022,15(23).
758 [33] C. Kang, Y.Q. Zhao, C. Tang, O. Addo-Bankas, Use of aluminum-based
759 water treatment sludge as coagulant for animal farm wastewater treatment,
760 *J. WATER. PROCESS. ENG.*, 2022, 46.
761 [34] L. Panda, P.K. Banerjee, S.K. Biswal, R. Venugopal, N.R. Mandre,
762 Modelling and optimization of process parameters for beneficiation of
763 ultrafine chromite particles by selective flocculation, *SEP. PURIF.*
764 *TECHNOL.*, 2014, 132: 666-673.
765 [35] R. Arjmand, M. Massinaei, A. Behnamfard, Improving flocculation and
766 dewatering performance of iron tailings thickeners, *J. WATER. PROCESS.*
767 *ENG.*, 2019, 31.
768 [36] S.H. Yin, Y.Q. Hou, S.X. Yang, X. Chen, Study on static and dynamic
769 flocculation settlement characteristics of fine tailings slurry and influence of
770 flocculant on strength of fine tailings backfill, *CASE. STUD. CONSTR. MAT.*,
771 2022, 17.
772 [37] C.C. Qi, H.B. Ly, Q.S. Chen, T.T. Le, V.M. Le, B.T. Pham, Flocculation-
773 dewatering prediction of fine mineral tailings using a hybrid machine
774 learning approach, *CHEMOSPHERE.*, 2020, 244.
775 [38] F.L. Motta, R. Gaikwad, L. Botha, J.B.P. Soares, Quantifying the effect of
776 polyacrylamide dosage, Na+ and Ca2+ concentrations, and clay particle
777 size on the flocculation of mature fine tailings with robust statistical methods,
778 *CHEMOSPHERE.*, 2018, 208: 263-272.
779 [39] F.S. Niu, H.M. Zhang, J.X. Zhang, X.D. Yu, W.B. Wang, Coagulation
780 sedimentation performance and model optimization of ultra-fine tailings
781 overflow from hydrocyclone, *MINER. ENG.*, 2022, 186.
782 [40] H. Puja, K. Shravan, Analysis of settling performance of coal fines tailing
783 polymer using central composite rotatable design optimization, *INT. J.*
784 *COAL. PREP. UTIL.*, 2019, 42(2).
785 [41] S.A. Musa, A.S. Abdulhameed, S.N.A. Baharin, Z.A. ALOthman, L.D.
786 Wilson, A.H. Jawad, Coal-Based Activated Carbon via Microwave-Assisted
787 ZnCl2 Activation for Methyl Violet 2B Dye Removal: Optimization,
788 Desirability Function, and Adsorption Mechanism, *MINERALS*, 2023, 13(3).
789 [42] M. Hasan, M. Rahman, Y. Chen, N. Cicek, Optimization of Typha Fibre
790 Extraction and Properties for Bio-Composite Applications Using Desirability
791 Function Analysis, *POLYMERS*, 2022,14(9).
792 [43] B.D. Clercq, P.A. Lant, P.A. Vanrolleghem, Focused beam reflectance
793 technique for in situ particle sizing in wastewater treatment settling tanks,
794 *J. CHEM. TECHNOL. BIOT.*, 2004, 79(6): 610-618.

[44] N. Kail, W. Marquardt, H. Briesen, Estimation of particle size distributions from focused beam reflectance measurements based on an optical model, *CHEM. ENG. SCI.*, 2009, 64(5): 984-1000.

[45] A.J.S. Cuthbertson, P. Dong, P.A. Davies, Non-equilibrium flocculation characteristics of fine-grained sediments in grid-generated turbulent flow, *COAST. ENG.*, 2010, 57(4): 447-460.

[46] P. Tang, J. Greenwood, J.A. Raper, A Model to Describe the Settling Behavior of Fractal Aggregates, *J. COLLOID. INTERF. SCI.*, 2002, 247(1): 210-219.

[47] W.A.S.K. Mancell-Egala, C.Y. Su, I. Takacs, J.T. Novak, D.J. Kinnear, S.N. Murthy, H.D, Clippeleir. Settling regimen transitions quantify solid separation limitations through correlation with floc size and shape, *WATER. RES.*, 2017, 109: 54-68.

[48] Z.H. Chai, J.Y. Lu, S.M. Yao, X. Wang, T.H. Liu, Modeling the growth of cohesive sediment flocs in three-dimensional space, Estuarine, *ESTUAR. COAST. SHELF. S.*, 2018, 215: 11-19.

[49] S. Sharma, C.L. Lin, J.D. Miller, Multi-scale features including water content of polymer induced kaolinite floc structures, *MINER. ENG.*, 2017, 101: 20-29.

Table S1 Asym2sig fitting parameter values and R^2 values corresponding to single flocculation factors

		l_0	t_c	A	w_1	w_2	w_3	R^2
PAM type	625S	33.556	7.566	253.751	9.393	1.117	34.533	0.977
	645S	29.253	5.066	653.819	3.752	1.472	117.620	0.961
	665S	50.632	22.699	136.437	33.419	0.005	22.500	0.933
	350E	-3.698	56.656	132.648	95.067	7.564	7.278	0.956
	6003S	51.124	31.470	315.727	50.977	0.023	45.279	0.946
FSC / wt%	5	23.967	103.514	352.916	200.251	1.309	92.688	0.979
	10	30.967	59.054	462.904	110.215	1.411	148.878	0.989
	15	2.574	5.648	676.031	1.402	2.350	160.39	0.976
	20	20.469	38.441	344.721	67.553	1.061	59.368	0.963
	25	35.775	3.649	401.457	1.204	0.831	48.144	0.967
TFC / wt%	0.01	-5.292	86.733	453.954	168.311	1.564	177.011	0.977
	0.0325	-20.718	74.120	373.040	144.716	1.176	48.649	0.991
	0.055	2.574	5.648	676.031	1.402	2.350	160.39	0.976
	0.0775	25.454	6.132	622.833	4.691	2.228	121.776	0.973

	0.1	26.968	60.173	297.792	109.818	1.016	37.540	0.985
	80	95.275	30.854	133.461	52.536	0.445	9.142	0.977
	160	44.359	48.076	347.881	83.633	1.193	79.492	0.991
SR / (r·min^{-1})	240	2.574	5.648	676.031	1.402	2.350	160.39	0.976
	320	39.511	9.866	419.410	12.093	0.469	40.147	0.973
	400	38.024	3.826	353.104	1.517	0.425	48.630	0.985
	30	25.548	62.046	376.676	114.787	1.487	73.194	0.993
	60	26.107	37.499	434.930	61.275	1.763	56.696	0.968
ST/ s	90	2.574	5.648	676.031	1.402	2.35	160.39	0.976
	120	-201.822	1.707	1031.788	5.904	4.943	254.436	0.875
	150	20.474	4.318	569.258	7.852	1.072	142.586	0.947

Table S2 Asym2sig fitting parameter values and R^2 values corresponding to RSM-BBD multi-factor experiments

No.	l_0	t_c	A	w_1	w_2	w_3	R^2
1	53.297	10.649	275.452	13.325	0.0153	50.980	0.974
2	-54.816	61.902	443.116	114.444	4.656	37.968	0.990
3	11.478	65.117	261.748	126.509	0.801	91.228	0.956
4	73.620	2.000	304.948	2.413	4.218	50.149	0.920
5	-131.227	0.565	826.086	4.166	5.883	181.086	0.970
6	66.25	18.416	216.020	29.287	0.00381	3.262	0.854
7	44.327	2.372	442.105	1.261	0.987	130.448	0.920
8	6.802	23.459	356.898	36.734	2.541	9.772	0.984
9	-142.141	15.570	862.447	24.092	5.788	86.908	0.980
10	41.841	21.49	267.794	33.968	0.798	2.696	0.982
11	49.609	8.170	305.177	1.108	1.255	32.265	0.963
12	42.482	23.704	249.701	39.452	0.0116	19.800	0.916
13	84.905	44.566	109.557	76.811	0.794	11.916	0.972
14	70.85	60.747	259.150	109.526	0.0299	51.661	0.891
15	28.445	4.191	668.848	3.278	1.374	122.034	0.943
16	37.835	4.170	629.174	9.072	1.219	144.405	0.942
17	9.039	42.032	312.770	70.992	4.492	22.793	0.986
18	30.759	2.906	159.990	2.716	1.488	70.388	0.936
19	22.274	4.430	625.044	1.589	1.062	66.248	0.972
20	28.445	4.191	668.848	3.278	1.374	122.034	0.943
21	47.606	9.135	380.512	1.938	1.778	64.849	0.985
22	28.445	4.191	668.848	3.278	1.374	122.034	0.943
23	53.426	10.349	143.733	16.681	0.00475	9.737	0.923
24	23.792	4.457	526.507	5.188	1.390	110.793	0.935
25	41.511	208.172	162.982	407.968	1.638	6.570	0.989
26	59.604	5.159	308.871	1.124	1.623	42.583	0.943
27	28.445	4.191	668.848	3.278	1.374	122.034	0.943

28	-18.615	6.385	680.644	2.521	5.433	91.616	0.985
29	79.671	5.922	343.187	2.561	1.316	34.411	0.955

820